# Implementation of A Low Cost Prototype for Electrical Impedance Tomography based on the Integrated Circuit for Body Composition Measurement AFE4300

Víctor Hugo Mosquera[1], Adrian Arregui[2], Ramon Bragós[2] and Carlos Felipe Rengifo[1]

[1]*Department of Electronic, University of Cauca, Street 5 # 4-70, Popayán, Colombia*

[2]*Department of Electronic Engineering, Technical University of Catalonia, Barcelona, Spain*

Keywords: Electrical Impedance Tomography, Image Reconstruction, Conductivity Distribution.

Abstract: Electrical impedance tomography (EIT) is a technique of image reconstruction of the electrical conductivity distribution in a tissue or region under observation. An electrical system for EIT comprises complex hardware and software modules, which are designed for a specific application which requires that the system to be able to detect conductivity variations within the study object. The Front-End for body composition measurement, AFE4300 from Texas Instruments allows a minimal implementation of an electrical impedance tomography system. It is the main device in the development of the EIT system presented in this paper, this device injects the current signal and measures the tensions generated on the study region boundary by 8 electrodes, the image reconstruction software was developed on the National Instruments platform Labview. The system includes a microcontroller PIC16F886 to configure the 8 channels for the definition of the patterns of injection and measurement of signals, also defines the current signal frequency and the bluetooth communication with the computer for the image reconstruction. The developed system was validated by a planar resistive phantom (CardiffEIT phantom), obtaining a stable voltage measurement every 50 ms per pair of electrodes, and a signal to noise ratio (SNR) maximum of 71.8 dB, for a current signal of 50 kHz. Additionally, tests were carried out in a saline tank with a concentration of 4 g/L, the developed system can simultaneously estimate the presence of conductive and non-conductive disturbances into the tank.

## 1 INTRODUCTION

Patients suffering from urological disease or spinal cord injury usually have difficulties perceiving bladder fullness and voiding due to neurological damage or muscular atrophy. If these patients do not empty their bladders on time, voiding dysfunction can result in urinary tract infections and urinary reflux, which may even lead to renal failure. The clinic process for bladder emptying is done by inserting a catheter into the bladder to drain urine, this method is invasive and may cause urinary tract infection, besides that not respect the micturition desire of patients. There are techniques that apply the ultrasound and pressure sensors for the bladder volume measurement for to assist the bladder emptying, with the disadvantages of the high noise and low precision of measurements (Li et al., 2016).

The impedance distribution measurement is another technique to measure the bladder volume with the aim of assisting the process of emptying bladder. Electrical impedance tomography (EIT) is a non-invasive technique that allows to get intra-thoracic images. The EIT systems are based on the injection of currents and on the measurement of the resulting potentials at the boundary, by means of electrodes. In EIT applications on biological tissues, the currents used are of sinusoidal nature, with amplitudes of a few *mA* and frequencies ranging from 1 and 100 kHz. Known the potentials and the currents at the object boundary to be analyzed, a method of image reconstruction is used to estimate the electrical conductivity distribution inside of the region (Harikumar et al., 2013).

The EIT has numerous applications in the medical field, successfully entering in the monitoring of intracranial hemorrhages or hematomas (Ayati et al., 2015), cancer detection (Gao et al., 2014), study of pelvic fluid accumulation (Li et al., 2016), pulmonary ventilation analysis (Bordes et al., 2016), blood pressure measurement (Proença et al., 2016), among others. The non-invasive and radiation-free character



Mosquera, V., Arregui, A., Bragós, R. and Rengifo, C.
Implementation of a Low Cost Prototype for Electrical Impedance Tomography based on the Integrated Circuit for Body Composition Measurement AFE4300.
DOI: 10.5220/0006554901210127
In *Proceedings of the 11th International Joint Conference on Biomedical Engineering Systems and Technologies (BIOSTEC 2018) - Volume 1: BIODEVICES*, pages 121-127
ISBN: 978-989-758-277-6

of the EIT makes this technique a good alternative for supporting the diagnosis and monitoring of medical pathologies (Harikumar et al., 2013), (Islam and Kiber, 2014).

Many studies have been advanced in the implementation of EIT systems, oriented to the detection and monitoring of medical pathologies, these works focus on the development of efficient and portable equipment, using electronic programmable devices. Within the studies developed we highlight the use of FPGA′s (*Field programmable Gate array*) or DSP′s (*Digital Signal Processors*), devices that allow to develop tomographic system capable of generating up to 50 images per second, which has promoted the use of EIT in problems with a high variation of the conductivity per unit of time, for example the monitoring of the blood pressure (Proença et al., 2016), (Balleza-Ordaz et al., 2015), (Bordes et al., 2016). For EIT systems oriented to medical applications with a low temporal variability of its conductivity, the use of microcontrollers presents good results as evidenced in (Chitturi et al., 2014), (Fouchard et al., 2014) and (Huang et al., 2016), with a lower cost compared to systems developed with DSP′s and FPGA′s. Applications such as the bladder emptying and studies of the cranial cavity and the bone system are fields in which low-frequency EIT systems can be used in processes of monitoring and pathologies detection (Li et al., 2016), (Atefi et al., 2016), (Ron et al., 2016).

The aim of this paper is to propose a new, low cost, 8 channels EIT system for rapid prototyping, intended for monitoring bladder emptying, process that need a low quantity of images per second, based on the body composition measurement device of Texas Instruments AFE4300. The hardware structure of the system is presented in section 2. The algorithm for the reconstruction of conductivity distribution images is described in section 3 and the experimental results in a saline tank are presented in section 4.

## 2 HARDWARE STRUCTURE

EIT systems require the injection of a sinusoidal current of both constant amplitude and frequency and also the measurement of the potential difference across the electrodes around the boundary of the object under study. The values of the injected current and the potentials measured on the electrodes are used as the inputs to the reconstruction algorithm, producing images of the electrical conductivity distribution. The system presented in this work generates a current signal of 833 $\mu$A at 50 kHz, which is injected by adjacent pairs of electrodes (Texas-Instruments, 2012). The measure of the potentials is carried out by using the adjacent electrode pairs method. These injection and measurement patterns can be modified by configuring the registers of the AFE4300.

The EIT system consists of a mixed front-end (AFE4300), which has 8 ports for current injection and 8 ports for potentials measurement, also integrates the direct digital synthesizer (DDS), voltage-controlled current source (VCCS), voltage sensing, quadrature demodulator or full-wave rectifier and the multiplexing stages for injection and measurement. The LabVIEW platform of National Instruments is used for the communication with the hardware and for the implementation of the image reconstruction algorithm. A microcontroller PIC16F886 connected to Bluetooth module HC06 is used as the interface between the PC running Labview and the AFE4300 based system. The block diagrams of the overall system is depicted in figure 1. A photograph of the card with the electronic components is presented in 2.

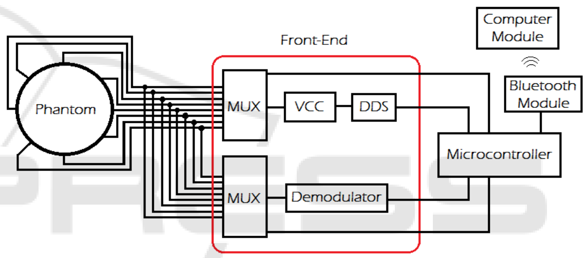


Figure 1: EIT system diagram.

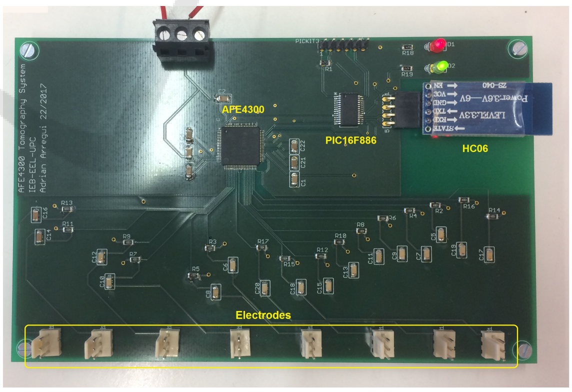


Figure 2: EIT system implemented.

### 2.1 Front-End AFE4300

To measure the body impedance, the AFE4300 generates a sinusoidal signal by means of a DDS. The frequency of this signal can be programmed from a 10-bit record. The DDS output signal feeds a 6-bit DAC whose refresh rate is 1 msps. The high-frequency components of the DAC output signal are eliminated by means of a low pass band second-order filter with a cut-off frequency of 150 kHz. The DC component of the signal delivered by the filter is removed by means of a in series external capacitor. One of the capacitor terminals is the input signal to a voltage-current converter that is connected to a multiplexer and then to the current injection ports (IOUTX). The injection pattern is programmed through the configuration register ISW_MUX. Figure 3 shows the scheme of body composition meter module of the AFE4300 described.

The voltage to current conversion is made through the following equation:

$$i(t) = \left(\frac{V_{AC}}{R_1}\right) \quad (1)$$

Being $R_1$ = 1.5 kΩ ± 20% an internal element of the AFE4300. Considering the minimal value of $R_1$, the maximal current generated is equal to the RMS value of the voltage $(1V_{pp}/(2\sqrt{2})$ divided by 1.2 kΩ, equivalent to 294.5 $\mu A$, which is below the maximum allowable current for a human being that is 500 $\mu A$ (Master and Mark, 2012).

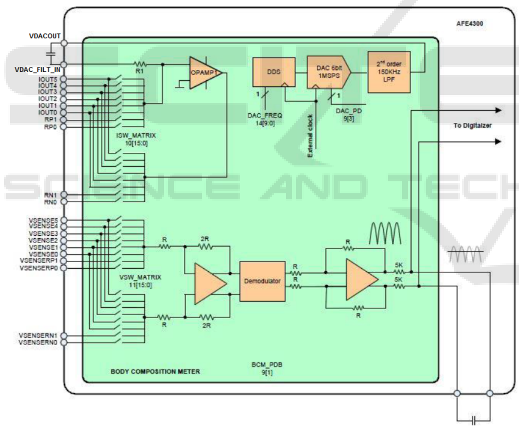


Figure 3: Front-End AFE4300 (Texas-Instruments, 2012).

The object to which the current signal is injected generates a voltage difference between the measuring electrodes, due to the internal conductivity distribution of the object. This voltage difference is sensed by the AFE4300 through the voltage ports (VSENSEx). Voltage measurements are performed using the adjacent electrode method, which is defined by the programming register VSENSE_MUX of AFE4300. Voltage measurements are entered into a differential amplifier, which determines voltage variation due to conductivity changes within the study object. This variation can be obtained by full wave rectification or by quadrature $(I/Q)$. The first option provides the magnitude of the impedance, while the second one generates the real and the imaginary parts of the impedance (Texas-Instruments, 2012). For this development the first measurement option is used, which after performing the full wave rectification, a low pass filter is used to generate a DC signal proportional to the impedance module $|Z|$ (Equation (2)).

$$V_{DC} = \frac{2}{T}\int_{T/2} A\,|Z|\,sin\,(\omega_0 t + \theta)\,dt = \frac{2A\,|Z|}{\pi} = K\,|Z| \quad (2)$$

$K$ is the proportionality constant due to calibration. For this study, the calibration ports of the device are not used, in order to have the availability of the 8 channels for the injection and measurement signals. The voltage values in the electrodes are sent to the PIC16F886, to be later transmitted via Bluetooth to the computer where the image reconstruction of the conductivity distribution is carried out.

As can be demonstrated, the system is of easy implementation and consists of a few number of electronic components, making this a compact and a portable system. Other EIT systems implemented with FPGA′s, DSP′s or microcontrollers, despite their promising results, are systems that involve several modules such as VCCS, Multiplexing, AD and DA converters and their respective interfaces, which makes these proposals, complex systems, such as those presented in (Bera and Nagaraju, 2009), (Khalighi et al., 2012) and (Wi et al., 2014).

The system designed is also low cost with a cost of 65.60€. The prices of the devices AFE4300, PIC16F886 and HC06 respectively are 4.58€, 2.09€ and 11.61€; passive elements such as resistors and capacitors, in addition to electrode connectors, 2000 mA LiPo 3.7 V battery and Power Cell LiPo Charger, have a price of 47.32€. Other systems based on FPGA Virtex or Ciclon (Santos et al., 2016), (Khan et al., 2015), (Shi et al., 2016) are more expensive as these devices exceed 280€, for which our proposal a more economical prototype.

## 3 IMAGES RECONSTRUCTION

The process of obtaining a conductivity distribution within the object from the current and voltage measurements on boundary is called the reconstruction algorithm. The reconstruction algorithms solve a mathematical problem that is nonlinear and ill-posed. There are several reconstruction methods, such as the absolute, dynamic and multifrequency (Santos and Simini, 2013). This work uses the dynamic method, which performs the reconstruction process from changes in conductivity, due to changes in the voltages in the electrodes, this technique is also known as differential image.

Considering that the injection and measurement are carried out in pairs of adjacent electrodes, it is possible to detect a voltage drop in any pair of electrodes. The gray region of the figure 4 shows the area whose changes in conductivity ($\delta\sigma$) generate changes over adjacent electrodes. These changes are a function of the measured voltages in different time or frequency and are estimated by the equation (3).

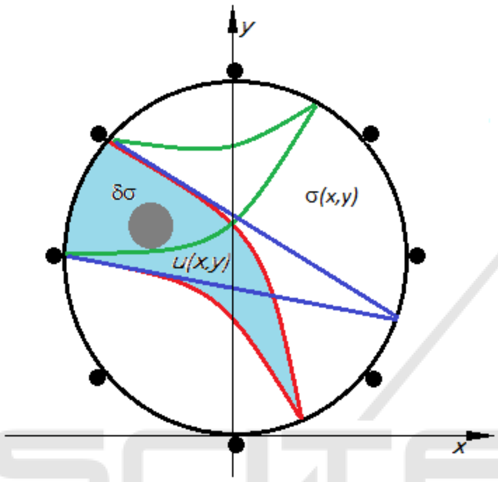


Figure 4: Conductivity changes Detection.

$$\delta\sigma(x,y) = -\frac{1}{N}\sum_{i=1}\Phi(u_k(t_0),u_k(t_0+\Delta t),\omega_i) \quad (3)$$

The change of conductivity $\delta\sigma$ by a pixel in a given position $(x,y)$ is estimated by the sum of the voltage changes ($\Phi$) produced in all the equipotential regions, defined by the measuring electrodes, where that pixel belongs. For each injection combination ($\omega_i$), one pixel will then belong only to one equipotential region $u_k$; For the implementation of the reconstruction algorithm is defined a weighting function $W(x,y,\omega_i)$, which is related to the conductivity sensitivity changes within the study object, then the mathematical model that describes the conductivity distribution is:

$$\delta\sigma = -\frac{1}{N}\sum_{i=1}\Phi\left(u_k\left(t_0\right),u_k\left(t_0+\Delta t\right),\omega_i\right)W\left(x,y,\omega_i\right) \quad (4)$$

The function $\Phi$ being calculated as:

$$\Phi(u_i(t_0),u_i(t_0+\Delta t),\omega_i) = ln(\frac{u_i(t_0+\Delta t)}{u_i(t_0)}) \approx \frac{u_i(t_0+\Delta t)-u_i(t_0)}{u_i(t_0)} \quad (5)$$

The reconstruction method represented by the equations (4) and (5) is implemented in C++ and compiled in a DLL (Dynamic Link Library), to later be used in a LabVIEW application.

## 4 EXPERIMENTAL TESTS

To verify the performance of the proposed EIT system the signal to noise ratio (SNR) is evaluated, this parameter estimates the precision of measurement, which quantified the repeatability of measurement under unchanged conditions. For the analysis of the SNR, a current signal of 50 kHz is injected into a 2D resistive phantom (Cardiff EIT Phantom). The SNR is calculated as the quotient between the mean and the standard deviation of each of the 30 measured frames. Different values of the delay between measures were tested 10, 25, 50 and 100 ms, with objective of to found the best characteristics the SNR. The results are presented in the table 1, which indicates that delay of 50 ms per measurement presents the best characteristics of SNR. This because of when switching a new channel, there is a transient that adds dispersion to the measurement if the delay between switching and acquiring is shorter than 25 ms. The dispersion improves if we wait for 50 ms, but it does not improve and even grows if the delay is 100 ms or more because there is a slow drift in the measured voltages that can be observed at the signal inputs, that is the reason of the dispersion increase for longer delays.

Table 1: SNR for different measurement times.

| | SNR (dB) | | |
|---|---|---|---|
| | **Maximum** | **Average** | **Minimum** |
| **10 ms** | 40.7 | 17.82 | 4.55 |
| **25 ms** | 74.73 | 28.57 | 9.74 |
| **50 ms** | 71.81 | 47.77 | 24.04 |
| **100 ms** | 56.04 | 45.7 | 33.95 |

Once the measurement time has been defined (50 ms), tests are carried out in a tank with a saline solution with conductive and non-conductive disturbances. The test for the image′s reconstruction begins by determining the conductivity distribution of the tank with the saline solution, with a concentration of salt of $4g/L$, in order to define the frame of reference for the dynamic reconstruction of subsequent images with the presence of disturbances. Once the reference frame is determined, conductive and non-conductive materials are inserted into the tank to evaluate the potential change over the surface electrodes.

In Figure 5 it is possible to observe the conductivity distribution within the tank without disturbances, in which small variations in the conductivity distribution can be observed.

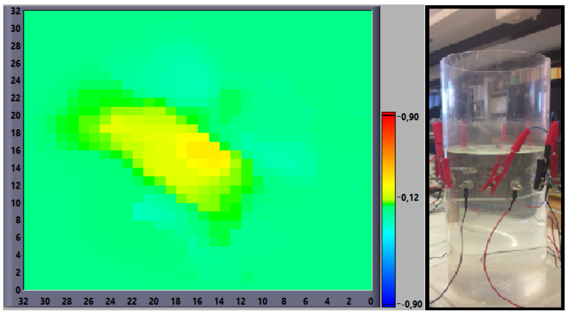

Figure 5: Reconstruction the conductivity distribution of the tank with saline solution.

Figure 6 shows the image reconstruction of the tank with a non-conductive disturbance (peek bar). From this Figure it can be observed that the object causes a disturbance that is represented by blue color due to a negative conductivity change of $-0.9$. The same procedure is carried out for a conductive disturbance object which generates a change of conductivity of $+0.9$ in the reconstructed image (Figure 7).

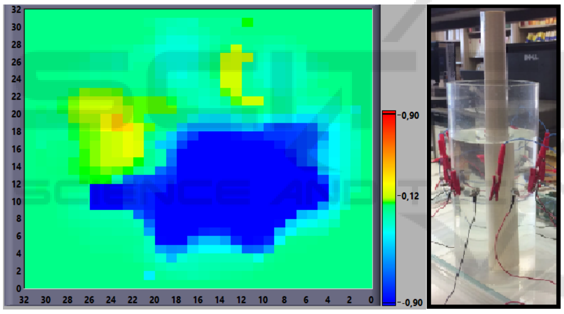

Figure 6: Reconstruction of conductivity distribution with non-conductive artefact.

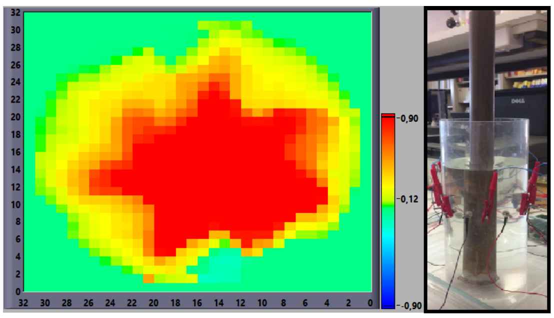

Figure 7: Reconstruction of conductivity distribution with conductive artefact.

Finally, the test is carried out with both a conductive and a non-conductive simultaneously, to evaluate the capacity of the proposed system to detect various types of disturbances. The figure 8 shows test result, in which the image clearly evidence the two objects of disturbance, discriminating between disturbances generated by the conductive and non-conductive materials.

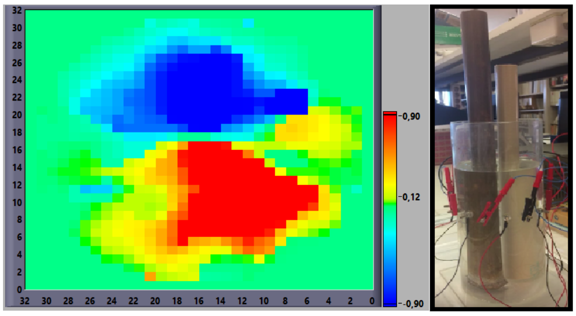

Figure 8: Reconstruction of conductivity distribution with non-conductive and conductive artefacts.

The results do not show good accuracy between the disturbance and the reconstructed image, which can be improved with a method to minimizing electrode interface impedance and a more elaborated image reconstruction algorithm. On the other hand, the system allows to detect changes in conductivity within a saline environment which makes this system a viable alternative to performing the study of slow physiological processes such as bladder emptying (Li et al., 2016), hematomas and hemorrhages studies (Aristovich et al., 2016).

The proposed system presents advantages over other developed devices because the AFE4300 concentrates the functions of: (i) electrical current generation, (ii) voltage measurement, (iii) multiplexing, and (iv) demodulation, reducing the modules of the system and its respective interfaces, facilitating its implementation at a low cost. Designs like the one presented in (Bera and Nagaraju, 2009), which employs a MAX038 for the generation of the current signal and a QuadTech7600 for the potential sensing, or in (Khalighi et al., 2012) that uses a XR2206 for waveform generation and a CD4067B for multiplexation, besides other modules, which makes the system a complex alternative to implement. On the other hand in (Wi et al., 2014) is presented a system called Khu Mark 2.5, is a fairly complex modular equipment that achieves 100 frames per second, but with a high economic cost.

## 5 CONCLUSION

The designed system has a maximum SNR of 71.81 dB, which allows detecting conductivity variations in a saline tank. The time delay of 50 ms between measurements makes this prototype a good alternative for the study of pathologies that do not require a high frames frequency.

The proposed system requires a few electronic components, which makes it easy to implement. On the other hand its characteristics can be improved by using more advanced methods of images reconstruction, which contribute to the decrease of the effects of the noise and to have a better SNR (Hadinia and Jafari, 2015), (Islam and Kiber, 2014).

## REFERENCES

Aristovich, K. Y., Packham, B. C., Koo, H., dos Santos, G. S., McEvoy, A., and Holder, D. S. (2016). Imaging fast electrical activity in the brain with electrical impedance tomography. *NeuroImage*, 124, Part A:204 – 213.

Atefi, S. R., Seoane, F., Kamalian, S., Rosenthal, E., Lev, M., and Bonmassar, G. (2016). Intracranial haemorrhage alters scalp potential distributions in bioimpedance cerebral monitoring applications : preliminary results from FEM simulation on a realistic head model and human subjects. *Medical Physics*, 43(2):675–686. QC 20170111.

Ayati, S. B., Bouazza-Marouf, K., and Kerr, D. (2015). In vitro localisation of intracranial haematoma using electrical impedance tomography semi-array. *Medical engineering & physics*, 37(1):34–41.

Balleza-Ordaz, M., Perez-Alday, E., Vargas-Luna, M., and Riu, J. (2015). Tidal volume monitoring by electrical impedance tomography (EIT) using different regions of interest (ROI): Calibration equations. *Biomedical Signal Processing and Control*, 18:102 – 109.

Bera, T. K. and Nagaraju, J. (2009). A Simple instrumentation calibration technique for Electrical Impedance Tomography (EIT) using a 16-electrode phantom. In *2009 IEEE International Conference on Automation Science and Engineering*, pages 347–352.

Bordes, J., Goutorbe, P., Cungi, P. J., Boghossian, M. C., and Kaiser, E. (2016). Noninvasive ventilation during spontaneous breathing anesthesia: an observational study using electrical impedance tomography. *Journal of Clinical Anesthesia*, 34:420 – 426.

Chitturi, V., Farrukh, N., Thiruchelvam, V., and Fei, T. K. (2014). A Low Cost Electrical Impedance Tomography (EIT) for Pulmonary Disease Modelling and Diagnosis. In *The Second International Conference on Technological Advances in Electrical, Electronics and Computer Engineering (TAEECE2014)*, pages 83–89. The Society of Digital Information and Wireless Communication.

Fouchard, A., Noca, A., Bonnet, S., Pham, P., Sinniger, V., Clarenon, D., and David, O. (2014). Modular architecture of a multi-frequency electrical impedance tomography system: Design and implementation. In *2014 36th Annual International Conference of the IEEE Engineering in Medicine and Biology Society*, pages 6076–6079.

Gao, J., Yue, S., Chen, J., and Wang, H. (2014). Classification of normal and cancerous lung tissues by electrical impendence tomography. *Bio-medical materials and engineering*, 24(6):2229–2241.

Hadinia, M. and Jafari, R. (2015). An element-free galerkin forward solver for the complete-electrode model in electrical impedance tomography. *Flow Measurement and Instrumentation*, 45:68–74.

Harikumar, R., Prabu, R., and Raghavan, S. (2013). Electrical impedance tomography (EIT) and its medical applications: a review. *Int J Soft Comp Eng*, 3(4):193–8.

Huang, J.-J., Hung, Y.-H., Wang, J.-J., and Lin, B.-S. (2016). Design of wearable and wireless electrical impedance tomography system. *Measurement*, 78:9–17.

Islam, M. R. and Kiber, M. A. (2014). Electrical impedance tomography imaging using gauss-newton algorithm. In *Informatics, Electronics & Vision (ICIEV), 2014 International Conference on*, pages 1–4. IEEE.

Khalighi, M., Vahdat, B. V., Mortazavi, M., Hy, W., and Soleimani, M. (2012). Practical design of low-cost instrumentation for industrial Electrical Impedance Tomography (EIT). In *Instrumentation and Measurement Technology Conference (I2MTC), 2012 IEEE International*, pages 1259–1263. IEEE.

Khan, S., Manwaring, P., Borsic, A., and Halter, R. (2015). FPGA-based voltage and current dual drive system for high frame rate electrical impedance tomography. *IEEE Transactions on Medical Imaging*, 34(4):888–901.

Li, R., Gao, J., Li, Y., Wu, J., Zhao, Z., and Liu, Y. (2016). Preliminary study of assessing bladder urinary volume using electrical impedance tomography. *Journal of Medical and Biological Engineering*, 36(1):71–79.

Master, T. and Mark, T. (2012). Medical electrical equipment part 1: General requirements for basic safety and essential performance.

Proença, M., Braun, F., Muntané, E., Solà, J., Adler, A., Lemay, M., Thiran, J.-P., and Rimoldi, S. F. (2016). Non-invasive monitoring of pulmonary artery pressure at the bedside. In *Engineering in Medicine and Biology Society (EMBC), 2016 IEEE 38th Annual International Conference of the*, pages 4236–4239. IEEE.

Proença, M., Braun, F., Solà, J., Thiran, J.-P., and Lemay, M. (2016). Noninvasive pulmonary artery pressure monitoring by EIT: a model-based feasibility study. *Medical & Biological Engineering & Computing*, pages 1–15.

Ron, A., Abboud, S., and Arad, M. (2016). Home monitoring of bone density in the wrista parametric EIT computer modeling study. *Biomedical Physics & Engineering Express*, 2(3):035002.

Santos, E. and Simini, F. (2013). Comparison of electrical impedance tomography reconstruction techniques applied to IMPETOM system. In *Bioinformatics and Bioengineering (BIBE), 2013 IEEE 13th International Conference on*, pages 1–4. IEEE.

Santos, S. A., Robens, A., Boehm, A., Leonhardt, S., and Teichmann, D. (2016). System Description and First

Application of an FPGA-Based Simultaneous Multi-Frequency Electrical Impedance Tomography. *Sensors (14248220)*, 16(8):1 – 21.

Shi, X., You, F., Xu, C., Ji, Z., Liu, R., Dong, X., Fu, F., and Huo, X. (2016). Design and implementation of a high-precision electrical impedance tomography data acquisition system for brain imaging. In *2016 IEEE Biomedical Circuits and Systems Conference (BioCAS)*, pages 9–15.

Texas-Instruments (2012). Datasheet-AFE4300-Low-Cost, Integrated Analog Front-End for Weight-Scale and Body Composition Measurement. *Dallas, Texas, USA*.

Wi, H., Sohal, H., McEwan, A. L., Woo, E. J., and Oh, T. I. (2014). Multi-frequency electrical impedance tomography system with automatic self-calibration for long-term monitoring. *IEEE transactions on biomedical circuits and systems*, 8(1):119–128.